Optimal and robust sizing of industrial solar powered microgrids with cloud passage resiliency constraints *

Louis Polleux[1,2], Sami Ghazouani[2], Gilles Guerassioff[1] Jean-Paul Marmorat[1]

[1] Center for Applied Mathematics, Mines Paristech, 06904 Sophia Antipolis, France
louis.polleux@mines-paristech.fr

[2] R&D hybrid program, TotalEnergies SE, 92400 La Défense, France
sami.ghazouani@totalenergies.fr

Abstract : *Intermittency of renewable resources brings new challenges for the optimal investment planning of industrial power systems. Reliability, availability, and power quality constraints force to strictly ensure the system's power balance during the operation. The risk of power quality degradation is increased with the integration of large-scale photovoltaic plants that face power variation due to cloud passage. If fossil generators cannot quickly compensate for the solar power drops, a fast-responding storage system must take over to guarantee electrical stability. Therefore, the sizing of industrial microgrid must integrate this storage system and consider cloud passage which modifies the techno-economic optimization paradigm. In this paper, sub-minute solar variability is anticipated thanks to robust scenarios and integrated within the optimization formulation. A linear power quality constraint is formulated to evaluate the storage needs for cloud passage resiliency. A case study is detailed and reports that short-term variability impacts the optimal solution due to additional storage costs.*

Keywords *: Linear-programming, Microgrids, Robust optimization, Solar Energy*

1 Introduction

Industrial processes electrification and renewable integration are being more and more investigated to reduce greenhouse gases emissions. However, in applications where no utility grid is available, industrial facilities must rely on on-site generation (microgrids) which brings lots of challenges related to electrical stability [2].

In previous work, the sizing of storage systems has been addressed thanks to dynamic models [1] requiring highly detailed grid description and large computational resources. However, in preliminary phases, industrial developers need a quick evaluation of techno-economic performances which led to investigate optimization based on high-level grid description.

In [4], a robust formulation has been proposed to size the power generation of microgrids but this work does not cover the resiliency over cloud passage. To address the electrical stability, the operational model of the optimization problem must embed frequency deviation constraints. This has been investigated in [3] thanks to non-linear optimization and benders decomposition but the author raised concerns about the computational complexity of this method. In addition, the frequency constrained formulations generally handle fossil generators contingency and do not address the problem of renewable's short term variations.

In previous work, we showed that storage system size depends on the level of variability of the photovoltaic (PV) power profile [6]. To avoid using 1-second resolution profiles that cannot be integrated in high-level energy models, the study proposed a method to identify isolated solar ramp scenarios.

This paper intends to propose a mixed integer linear programming (MILP) formulation for the optimal and robust sizing of industrial microgrids by considering robust solar variability

*Preprint submitted to ROADEF2022 Conference : https://roadef2022.sciencesconf.org

scenarios and a linear stability constraint. In section 2, the MILP sizing problem is detailed. Then, the robust management of cloud passage and its integration within the optimisation problem are addressed in section 3. A case study is detailed in section 4. Finally, conclusions are drawn in section 5.

2 Optimal sizing problem

The initial formulation of the power plant sizing is formulated in this section. Symbols of the form $\dot{x}$ refer to the decision variables. The optimization aims to find the best performing pair of PV and battery installed capacities respectively denoted $\dot{Q}_{PV}^{inst}$ and $\dot{Q}_{bat}^{inst}$. Eq. (1) shows the objective function with c_{PV} and c_{bat} being the installation costs of PV and battery systems (in $\$.kW^{-1}$) and c_f referring to the aggregated fuel costs including CO_2 penalty. The operating costs are calculated at each hourly time step of the year (8760 steps) and over the lifetime Y_{inst} (in years) thanks to operational decision variables on fossil unit m at each timestep h : the fuel consumption $\dot{FC}_{h,m}$, the unit power $\dot{P}_{h,m}$ the binary operating status $\dot{\omega}_{h,m}$, the binary unit start-up and shut down decisions $\dot{u}_{h,m}$ and $\dot{v}_{h,m}$. Additionally, $\dot{Q}_{PV_h}^{used}$ and $\dot{P}_{PV_h}^{inj}$ respectively denote the decision variables for hourly PV available capacity after curtailment and hourly injected PV power.

$$f = \dot{Q}_{PV}^{inst} * c_{PV} + \dot{Q}_{bat}^{inst} * c_{bat} + Y_{inst} * \sum_{h=1}^{8760} \sum_{m} (\dot{FC}_{h,m} * (c_f)) \tag{1}$$

Eq. (2) to (12) express the system operational constraints as formulated and detailed in [5]. Eq. (2) ensures that the hourly load demand P_l is satisfied. The injected PV power is calculated in Eq. (3) thanks to the hourly averaged irradiance I_h and PV derating factor d_{PV}. Eq. (4) ensures that the hourly curtailed PV capacity is lower that the PV installed capacity. Eq. (5) to (8) express the fossil generators operational constraints where P_m^{max} and P_m^{min} denote the parameters for maximum and minimum power ratings and M_m^{up} and M_m^{dn} denote the parameters for minimum up and down time of the fossil unit. The fuel consumption are evaluated thanks to the fuel curve's linear interpolation parameters a_m and b_m in Eq. (11).

$$\forall h, \quad \sum_{m} \dot{P}_{h,m} + \dot{P}_{PV_h}^{inj} - Pl_h \geq 0 \tag{2}$$

$$\forall h, \quad \dot{P}_{PV_h}^{inj} \leq \dot{Q}_{PV_h}^{used} * I_h * d_{PV} \tag{3}$$

$$\forall h, \quad \dot{Q}_{PV_h}^{used} \leq \dot{Q}_{PV}^{inst} \tag{4}$$

$$\forall h, m \quad \dot{P}_{h,m} \leq P_m^{max} * \dot{\omega}_{h,m} \tag{5}$$

$$\forall h, m \quad \dot{P}_{h,m} \geq P_m^{min} * \dot{\omega}_{h,m} \tag{6}$$

$$\forall h, m \quad \dot{u}_{h,m} - \dot{v}_{h,m} \geq \dot{\omega}_{h,m} - \dot{\omega}_{h-1,m} \tag{7}$$

$$\forall h, m \quad \dot{u}_{h,m} + \dot{v}_{h,m} \leq 1 \tag{8}$$

$$\forall m, \forall h \geq M_m^{up}, \quad \sum_{k=h-M_m^{up}}^{h-1} \dot{\omega}_{k,m} - M_m^{up} * \dot{v}_{h,m} \geq 0 \tag{9}$$

$$\forall m, \forall h \geq M_m^{dn}, \quad M_m^{dn} * (1 - \dot{u}_{h,m}) - \sum_{k=h-M_m^{dn}}^{h-1} \dot{\omega}_{k,m} \geq 0 \tag{10}$$

$$\forall h, m \quad \dot{FC}_{h,m} = a_m \dot{P}_{h,m} + b_m \tag{11}$$

Eq. (12) and (13) ensures that fossil generators can compensate variations ΔI_h^{avg} between the hourly average PV power and its minimum value. The decision variable $\Delta \dot{P}_{h,m}^{avg}$ denotes the generator spinning reserve allocated to these variations.

$$\forall h \quad \Delta I_h^{avg} \dot{Q}_{PV_h}^{used} \leq \sum_m \Delta \dot{P}_{h,m}^{avg} \tag{12}$$

$$\forall h, m \quad \Delta I_h^{avg} \dot{Q}_{PV_h}^{used} \leq \dot{\omega}_{h,m} P_m^{max} - \dot{P}_{h,m} \tag{13}$$

3 Robust management of cloud passage

3.1 A linear constraint to ensure power quality during cloud passage

The formulation detailed in section 2 ensures that the load balance is satisfied if PV power variations happen. But in case of fast cloud passage, fossil generators cannot instantaneously compensate the PV drop. This comes from the limited ramping capacities of fossil generators rr_m (in $MW.s^{-1}$) as compared to solar variations. The system's equation of motion is expressed in Eq. (14) where ΔP refers to incremental power variations of devices, M denotes the system's mechanical inertia and D refers to the system's load damping constant. From Eq. (14), frequency drops are expected to happen if PV power variations are not balanced. If the grid frequency drops bellow a given minimum value, power producers and consumers must disconnect to avoid a complete blackout and potential safety issues. Since Eq. (14) gives a non-linear relationship between power unbalances and frequency shift, a linear approximation of the system must be performed to allow its integration within the MILP problem.

$$\frac{d\Delta f}{dt} = \frac{\Delta P_{fossil} + \Delta P_{bat} + \Delta P_{PV} - \Delta P_l + D\Delta f}{M} \tag{14}$$

By assuming a linear power supply over time by fossil, battery and PV systems, Eq. (15) formulates a linear constraint which ensures that no frequency shift will happen during a PV drop of magnitude ΔP_{PV}^{fc} and duration ΔT^{fc} . The power adequacy is guaranteed by allocating enough storage capacity P_{bat}^{fc}. The battery reaches its maximum power at $t = \Delta T^{fc}$ which gives a lower bound for the storage capacity requirement.

$$P_{bat}^{fc} = \Delta P_{PV}^{fc} - \Delta T^{fc} \sum_m \dot{\omega}_m * rr_m \tag{15}$$

3.2 Cloud passage scenarios

Now that a linear constraint has been formulated, solar variability scenarios must be defined to cover the risk of PV drop. The challenge of such task is to aggregate and extract isolated ramp events from daily timeseries to allow their integration in a high level energy model. This is done by finding worst-cases pairs of PV drop duration ΔT^{fc} and magnitude ΔP_{PV}^{fc}. By processing irradiance timeseries by the ramp-detection technique detailed in [6], all solar drops have been identified. Figure 1 reports an example of this process on a daily irradiance timeseries.

To find the worst-case events among all detected ramps, a convex hull $\mathcal{H}^{max}$ is formed by the set of highest irradiance drops as shown in figure 2a. This gives a first robust approach to generate solar variability scenarios. Figure 2a is revealing that the maximum drop within $\mathcal{H}^{max}$ reaches 1.09 kW/m^2. If the frequency constraint is similarly evaluated for each hour of the day, risks of solar drop will be highly overestimated for hours of low irradiance.

An alternative to global convex hull consists in using hourly convex hulls $\mathcal{H}_h^{max}$. These sets are formed by the worst ramp detected at each hour of the day. In this case, the maximum solar drop between 7am and 8am is 0.44 kW/m^2 whereas it reaches 1.09 kW/m^2 between 11am

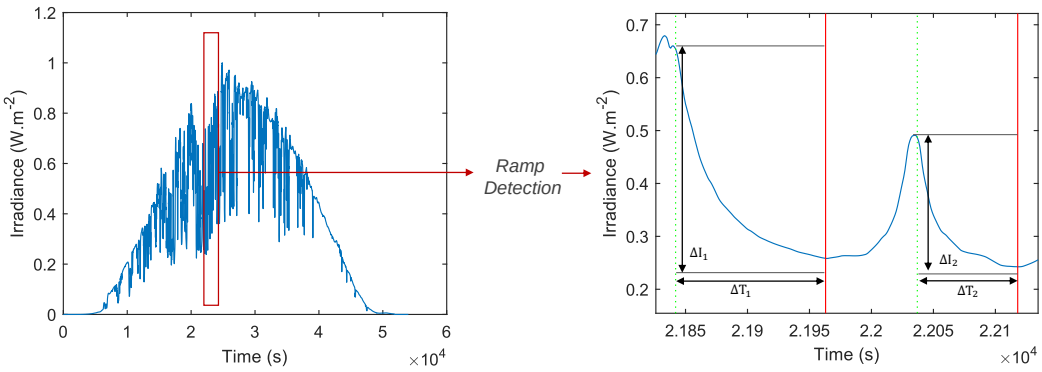

FIG. 1: Pre-processing of irradiance timseries to identify irradiance drops

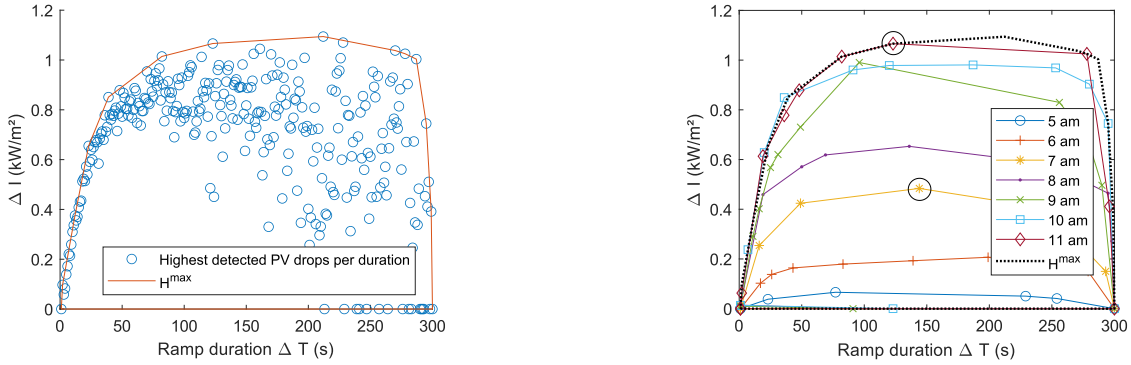

(a) (b)

FIG. 2: (a) : Global convex hull $\mathcal{H}^{max}$ formed by highest irradiance drop. (b): hourly convex hulls $\mathcal{H}_h^{max}$ corresponding to morning hours

and 12am (highlighted by black circles in figure 2b). Therefore, risks of frequency drops are evaluated with more accuracy and are not overestimated.

3.3 Integration within optimization problem

A static frequency constraint (Eq. (15)) have been proposed in the previous section and must now be integrated in the optimization problem to ensure the system's resiliency to cloud passage. $\dot{P}_{bat_h}^{fc}$ denotes the hourly storage power that must be available to ensure cloud passage compensation. The frequency constraint is expressed for all elements $r = (\Delta I_r^{fc}, \Delta T_r^{fc})$ either within the global hull ($r \in \mathcal{H}^{max}$) or hourly hull ($r \in \mathcal{H}_h^{max}$).

$$\forall h, r \quad \Delta \dot{P}_{PV_r}^{fc} = \dot{Q}_{PV}^{inst} \Delta I_{h,r}^{fc} * d_{PV} \tag{16}$$

$$\forall h, \quad \dot{Q}_{bat}^{inst} \geq \dot{P}_{bat,h}^{fc} \tag{17}$$

To integrate the frequency constraint in the LP formulation, the cloud passage event is divided in two main steps : the cloud passage (DC) and post-cloud state (PC).

Cloud passage phase In the cloud passage phase (denoted as DC), the frequency constraint must be satisfied thanks to Eq. (18). $\Delta \dot{P}_{h,m,r}^{DC}$ denotes the contribution of fossil generator (m) at the end of the cloud passage. Eq. (19) ensures that the fossil units do not violate their maximum

ramp-rates whereas Eq. (20) ensures that fossil generators do not meet their maximum power ratings at the end of the cloud passage.

$$\forall h, r \quad \Delta \dot{P}^{fc}_{PV_{h,r}} \leq \dot{P}^{fc}_{bat_h} + \sum_m \Delta \dot{P}^{DC}_{h,m,r} \tag{18}$$

$$\forall h, m, r \quad \Delta \dot{P}^{DC}_{h,m,r} \leq T_r * rr_m \tag{19}$$

$$\forall h, m, r \quad \Delta \dot{P}^{DC}_{h,m,r} \leq \dot{\omega}_{h,m} P^{max}_m - \dot{P}_{h,m} \tag{20}$$

Post-cloud passage phase At the end of the post-cloud step, the battery should not provide any power. Thus, fossil generator must keep increasing to reach a new equilibrium (secondary frequency support). The PV gap $\Delta \dot{P}^{fc}_{PV_{h,r}}$ must be solely filled by the fossil generation leading to Eq. 21. $\Delta P^{PC}_{h,m,r}$ denotes the contribution of the machine to the cloud compensation at the end of the post-cloud state. Eq. (22) ensures that enough spinning reserve is available.

$$\forall h, m, r \quad \Delta \dot{P}^{fc}_{PV_{h,r}} \leq \sum_m \Delta \dot{P}^{PC}_m \tag{21}$$

$$\forall h, m, r \quad \Delta \dot{P}^{PC}_{h,m,r} \leq \dot{\omega}_{h,m} P^{max}_m - \dot{P}_{h,m} \tag{22}$$

4 Case Study

The optimal sizing formulation is tested on a case study composed of 4 gas turbines and a constant load profile of 130MW. The main input parameters are summarized in table 1. Four cases are evaluated : in the "base case", no PV is considered which gives a reference for the system without PV penetration. In the "No-FC" case, no frequency constraint is considered. Frequency constraint is activated in "FC-global" and "FC-hourly" cases with worst case ramps taken from global convex hull and hourly hulls respectively.

Category	Name	Symbol	Unit	Value
Project	Lifetime	Y^{inst}	Year	20
Fossil generation	Ramp rate	rr_m	$MW.s^{-1}$	208
	Fuel curve slope	a	$m^3.h^{-1}.kW^{-1}$	13782
	Fuel curve intercept	b	m^3	5523
	Fuel price	c_{fuel}	$\$.mbtu^{-1}$	20
PV system	Capex	c^{inst}_{PV}	$\$.kW^{-1}$	600
	Derating factor	d_{PV}	%	80
Storage system	Capex	c^{inst}_{PV}	$\$.kW^{-1}$	400

TAB. 1: Techno-economic input parameters

Table 2 presents the results of the optimization. The base case reports the highest total costs. The minimal costs is found for the "NO-FC" case thanks to 196.9 MW of PV installed capacity. The CO_2 emission is reduced by 16.7% as compared to the base case. However, this solution not realistic since it does not take fast cloud passage into account : in this configuration, a solar ramp of 0.65 $kW.m^{-2}$ over 23 seconds (see figure 2b) would cause a power drop of 46MW and lead to an electrical blackout. Activating the frequency constraint leads to a reduction of PV capacity due to battery investments. In the "FC-global" case, the optimal solution gives a PV installed capacity of 2.6MW which results in 0.24% of CO_2 reduction. In the "FC-hourly" case, the PV installed capacity reaches 67.1 MW and leads to 4.8% of CO_2 savings.

Results show that activating frequency constraint leads to a reduction of PV installed capacity. If the global convex hull is used, PV risks are overestimated and the battery need becomes

so high that fuel savings are not worth the investment in storage system. This supports the interest of refining variability scenarios by considering convex hulls to improve the solution.

	Base Case	No FC	FC-global	FC-hourly
Total costs (B$)	4,95	4,24	4,93	4,76
Capex (m$)	0,0	118,1	1,5	49,5
Fuel OPEX (m$/year)	247	206	246	235
CO2 (mtons/year)	804	669	801	765
PV capacity (MW)	0,0	196,9	2,6	67,1
Battery capacity (MW)	0,0	0,0	0,0	23,2

TAB. 2: Results of sizing optimization

5 Conclusion

In this paper, a procedure to address short term variability in the sizing of industrial microgrids is proposed. A linear power quality constraint is formulated and ensures that no frequency shift appears during a PV power drop. Thanks to the detection of highest solar drops among an irradiance dataset, worst case ramp scenarios are gathered in convex hulls. Then, the frequency constraint is evaluated for each element of the worst case set. The case study showed that considering frequency constraint with the most robust strategy significantly reduce the PV installed capacity as compared to the standard formulation (2.6MW against 196.9MW). Using hourly hulls improves the solution and leads to 4.8% of CO_2 savings instead of 0.24%. Thus, this method avoids over-estimating the power plant performances and ensures that operators will not face electrical stability problems. A perspective is to formulate a stochastic optimization problem integrating solar drop probabilities and offer a larger potential for PV integration.

References

[1] Erick Alves, Santiago Sanchez, Danilo Brandao, and Elisabetta Tedeschi. Smart Load Management with Energy Storage for Power Quality Enhancement in Wind-Powered Oil and Gas Applications. *Energies*, 12(15):2985, August 2019.

[2] Atle Rygg Ardal, Kamran Sharifabadi, Oyvind Bergvoll, and Vidar Berge. Challenges with integration and operation of offshore oil & gas platforms connected to an offshore wind power plant. In *2014 Petroleum and Chemical Industry Conference Europe*, pages 1–9, Amsterdam, Netherlands, June 2014. IEEE.

[3] Carmen Cardozo Arteaga. *Optimisation of power system security with high share of variable renewables: Consideration of the primary reserve deployment dynamics on a Frequency Constrained Unit Commitment model.* Thèse de doctorat, Univertié Paris-Saclay, Paris, France, March 2016.

[4] Paolo Gabrielli, Florian Fürer, Georgios Mavromatidis, and Marco Mazzotti. Robust and optimal design of multi-energy systems with seasonal storage through uncertainty analysis. *Applied Energy*, 238:1192–1210, March 2019.

[5] Daniel E. Olivares, Claudio A. Canizares, and Mehrdad Kazerani. A Centralized Energy Management System for Isolated Microgrids. *IEEE Transactions on Smart Grid*, 5(4):1864–1875, July 2014.

[6] Louis Polleux, Thierry Schuhler, Gilles Guerassimoff, Jean-Paul Marmorat, John Sandoval-Moreno, and Sami Ghazouani. On the relationship between battery power capacity sizing and solar variability scenarios for industrial off-grid power plants. *Applied Energy*, 302:117553, November 2021.